

Month-Long Simulations of Gravity Waves over North America and North Atlantic in Comparison with Satellite Observations

ZHANG Fuqing^{1*} (张福青), ZHANG Meng^{1,3} (张盟), WEI Junhong¹ (卫俊宏),

and WANG Shuguang² (汪曙光)

¹ Department of Meteorology, Pennsylvania State University, University Park, PA 16802, USA

² Department of Applied Physics and Applied Mathematics, Columbia University, New York, NY 10027, USA

³ IBM Research, Beijing 100101, China

(Received December 10, 2012; in final form March 30, 2013)

ABSTRACT

Mesoscale simulations of gravity waves in the upper troposphere and lower stratosphere over North America and North Atlantic Ocean in January 2003 are compared with satellite radiance measurements from the Advanced Microwave Sounding Unit-A (AMSU-A). Four regions of strong gravity wave (GW) activities are found in the model simulations and the AMSU-A observations: the northwestern Atlantic, the U.S. Rockies, the Appalachians, and Greenland. GWs over the northwestern Atlantic Ocean are associated with the midlatitude baroclinic jet-front system, while the other three regions are apparently related to high topography. Model simulations are further used to analyze momentum fluxes in the zonal and meridional directions. It is found that strong westward momentum fluxes are prevalent over these regions over the whole period. Despite qualitative agreement between model simulations and satellite measurements, sensitivity experiments demonstrate that the simulated GWs are sensitive to the model spin-up time.

Key words: gravity wave, satellite radiance measurement, baroclinic jet-front

Citation: Zhang Fuqing, Zhang Meng, Wei Junhong, et al., 2013: Month-long simulations of gravity waves over North America and North Atlantic in comparison with satellite observations. *Acta Meteor. Sinica*, **27**(3), 446–454, doi: 10.1007/s13351-013-0301-x.

1. Introduction

Gravity waves (GWs) are one of the most fundamental dynamical processes in the atmosphere. Their generation, propagation, and breaking have profound impact on general circulations and climate (Fritts and Alexander, 2003; Plougonven and Zhang, 2013). It is now known that GWs can be generated by a variety of processes in the lower troposphere, including topography, convection, shear instability and/or geostrophic adjustment associated with baroclinic jet-front systems (e.g., Blumen and Wu, 1995; Zhang et al., 2001). GWs from these processes often have horizontal wavelengths of 50–500 km and intrinsic periods of 0.5–4 h (Uccellini and Koch, 1987). Because of their transient nature, these waves are difficult to

observe by conventional observations and to resolve by coarser-resolution numerical models (Plougonven and Zhang, 2013). While it is now well appreciated that the drag effect by GWs is vital for global momentum budget, progress toward better GW parameterization is severely limited by the lack of high resolution observations and numerical modeling (Kim et al., 2003).

Complementary to limited in-situ observations, satellite measurements have been proved to be useful in detecting GW activities with considerable resolution and coverage, especially over mountainous and oceanic areas, and in the upper atmosphere (Alexander et al., 2010; Plougonven and Zhang, 2013). For example, variance of the radiance from the Advanced Microwave Sounding Unit-A (AMSU-A) may reflect the temperature perturbations produced by GWs

Supported by the United States NSF Grants ATM-0618662 and ATM-0904635.

*Corresponding author: fzhang@psu.edu.

©The Chinese Meteorological Society and Springer-Verlag Berlin Heidelberg 2013

(Wu, 2004). In the meantime, ever-increasing computing resources begin to allow more realistic and comprehensive representations of GWs in complex, high-resolution mesoscale models (e.g., Zhang, 2004). The first attempt to simulate an observed gravity wave event was published in Powers and Reed (1993). Based on a successful simulation of a large-amplitude GW event over the northeastern United States, Zhang et al. (2001, 2003) discussed the mesoscale dynamics associated with the GW's radiation, maintenance, and amplification.

By comparing satellite-based observations with numerical simulations, Wu and Zhang (2004) first demonstrated the use of the AMSU-A microwave data to investigate GW activities associated with the tropospheric baroclinic jet-front systems over the northeastern United States and the North Atlantic in the December–January periods. They showed the observational evidence of GWs reaching the stratosphere with growing amplitude in the storm-track exit region. In particular, they documented the detailed analysis of a strong jet-front GW episode observed during 19–21 January 2003. They further showed that the simulated GWs with a mesoscale weather prediction model compare qualitatively well with the satellite observations in terms of wave structures, timing, and overall morphology.

As a follow up of Wu and Zhang (2004), and complementary to Shutts and Vosper (2011) who showed that a state-of-the-art global weather prediction model was capable of capturing the overall observed strength and distribution of GW activities derived from the High-Resolution Dynamics Limb Sounder (HIRDLS), the current study will use a mesoscale model to simulate GWs over North America and North Atlantic Ocean throughout the month of January 2003, when the westerly tropospheric jets are strong. The mesoscale simulations are compared with the AMSU-A estimated temperature variations in the lower stratosphere, and subsequently used to identify wave source regions and vertical structure, and to estimate vertical momentum transport. Sensitivity of wave simulations to lead time and model resolutions will also be discussed.

2. Datasets and analysis procedure

As in Wu and Zhang (2004), the Penn State University-NCAR mesoscale model 5 (MM5) (Grell et al., 1994) is employed in this study to simulate the GW activities over North America and North Atlantic Ocean. A single domain adopting 300×200 horizontal grid points and 30-km spacing is built over 90 vertical levels up to 10 hPa (about 28 km). The top 4-km layer is used as the gravity wave absorption layer to prevent artificial wave reflection from the model top. To avoid synoptic-scale climate drift in long-term integration of regional models, we performed a series of short-term MM5 integrations; each initialized at every 0000 UTC and integrated for 54 h. We find that the GW signals appear to saturate after a 30-h spin-up (details in Section 5), and we only use the last 24 hours for the analysis of GWs.

The initial and lateral boundary conditions are interpolated from the analysis data on a $2.5^\circ \times 2.5^\circ$ resolution, provided by the European Centre for the Medium-Range Weather Forecasts (ECMWF). For all simulations, we use the following physics parameterization schemes: the Grell cumulus parameterization scheme, mixed-phase microphysics scheme, and medium-range forecast (MRF) planetary boundary layer (PBL) parameterization scheme. Sensitivity experiments with a finer grid spacing (10 km) are conducted during a major jet-front GW event during 18–25 January 2003 to test the model capability of resolving GWs at different wavelengths.

The perturbation kinetic energy (KE) is chosen as a measure of GW activity and defined as (Allen and Vincent, 1995; Sato et al., 1999):

$$\text{KE} = \frac{1}{2}(\overline{u'^2} + \overline{v'^2} + \overline{w'^2}), \quad (1)$$

where u' , v' , and w' are the perturbation wind components. A two-dimensional band-pass filter is used to extract perturbations. We will focus on GWs with horizontal wavelengths between 200 and 600 km, which can be resolved by both the AMSU-A measurements and the model simulations. The monthly mean and

segment-averaged values of KE are then calculated over selected areas.

Three AMUS-A cross-track scanning instruments operated by the U.S. National Oceanic and Atmospheric Administration (NOAA) are used, i.e., NOAA-15, NOAA-16, and NOAA-17. Including both the ascending and descending scans by these three instruments, the North America and North Atlantic regions are sampled every 4 h (or 6 times per day). The scan swath is about 2300 km with footprint size between 50 and 110 km from nadir to outermost. There are totally 15 sounding channels for AMSU-A instrument, 6 of which (channels 9–14) have the temperature weighting function peaked at 18, 21, 26, 33, 38, and 45 km, respectively. The others (channels 1–8 and 15) are not used in this study, considering the larger impacts of surface emission and cloud scattering. The data processing and quality control of the AMSU-A observations are conducted based on the methods described in Wu and Zhang (2004), where the background radiance is filtered out by a horizontal nine-point running window.

It is worth noting that the AMSU-A radiances are sensitive to mesoscale gravity waves of longer vertical wavelength (> 10 km; Wu, 2004). The vertical resolution of the radiance variance, instead of being determined by the number of sounding channels used, is limited by the thickness of temperature weighting function (Wu and Zhang, 2004). Given the limited model top height (28 km) for the regional scale model used in the current study, and the limitation in the thickness of the vertical weighting function, it is very difficult (if not impossible) to obtain direct comparison of the simulations and observations at the same part of the spectrum. For the example case examined in Wu and Zhang (2004), the characteristic vertical scales of the GWs are 7–15 km in the simulation versus 20–30 km in the AMSU-A radiance. Despite this mismatch, there is qualitatively good agreement in the variances between the AMSU-A retrieval and the model simulation.

3. Comparisons between simulated and observed GWs

The GW KE is calculated every 3 h and averaged

over the month-long period. Figure 1a shows its spatial pattern in the lower stratosphere (21 km), along with the mean flow at the jet-core level (12 km). Four regions of significant GW activities can be identified: the northwestern Atlantic, the U.S. Rockies, the Appalachians, and Greenland, which will be referred to as Regions I, II, III, and IV, respectively, in the following text. Regions II, III, and IV are characterized by high topography, thus enhanced GW activities over these regions are likely generated by topographic sources (Fritts and Nastrom, 1992). On the other hand, considerable GW activities over the northwestern Atlantic (Region I) are found along the left flank of the upper-level jet exit region, which is also referred to as the Atlantic storm-track often associated with strong surface front and moist convections. The occurrence of enhanced GW activities over Region I appears to be consistent with observational composite (Uccellini and Koch, 1987) and several idealized numerical experiments (e.g., Zhang, 2004).

To verify the model-derived GWs, the monthly mean variance of AMSU-A radiance at approximately 21-km equivalent (channel 10) is shown in Fig. 1b, overlapped with the mean flows from the NCEP FNL analysis. Comparing Figs. 1a with 1b indicates that model simulated time mean upper-level jet (dashed curves) compares well with the mean FNL analysis. GW activities also agree well with the AMSU-A radiance over Regions I and III. The largest discrepancy between the model KE and the satellite variance is found over the Regions II and IV (Fig. 1a vs. Fig. 1b), where the modeled GWs are stronger than satellite radiance variations over the Rockies but weaker over Greenland. Underestimation in Region I is likely because a large portion of variance in the model comes from small scale (both horizontal and vertical) complex topography of the Rockies (Region II), which generates abundant smaller scale disturbances that cannot be resolved by the AMSU-A radiance. Underestimation over Region IV might be due to a weaker bias in the cross mountain flow over the Greenland high topography.

Figure 2 shows the temporal and vertical variations of GW activities over the four selected regions. The local mean of KE is each calculated over a 1200

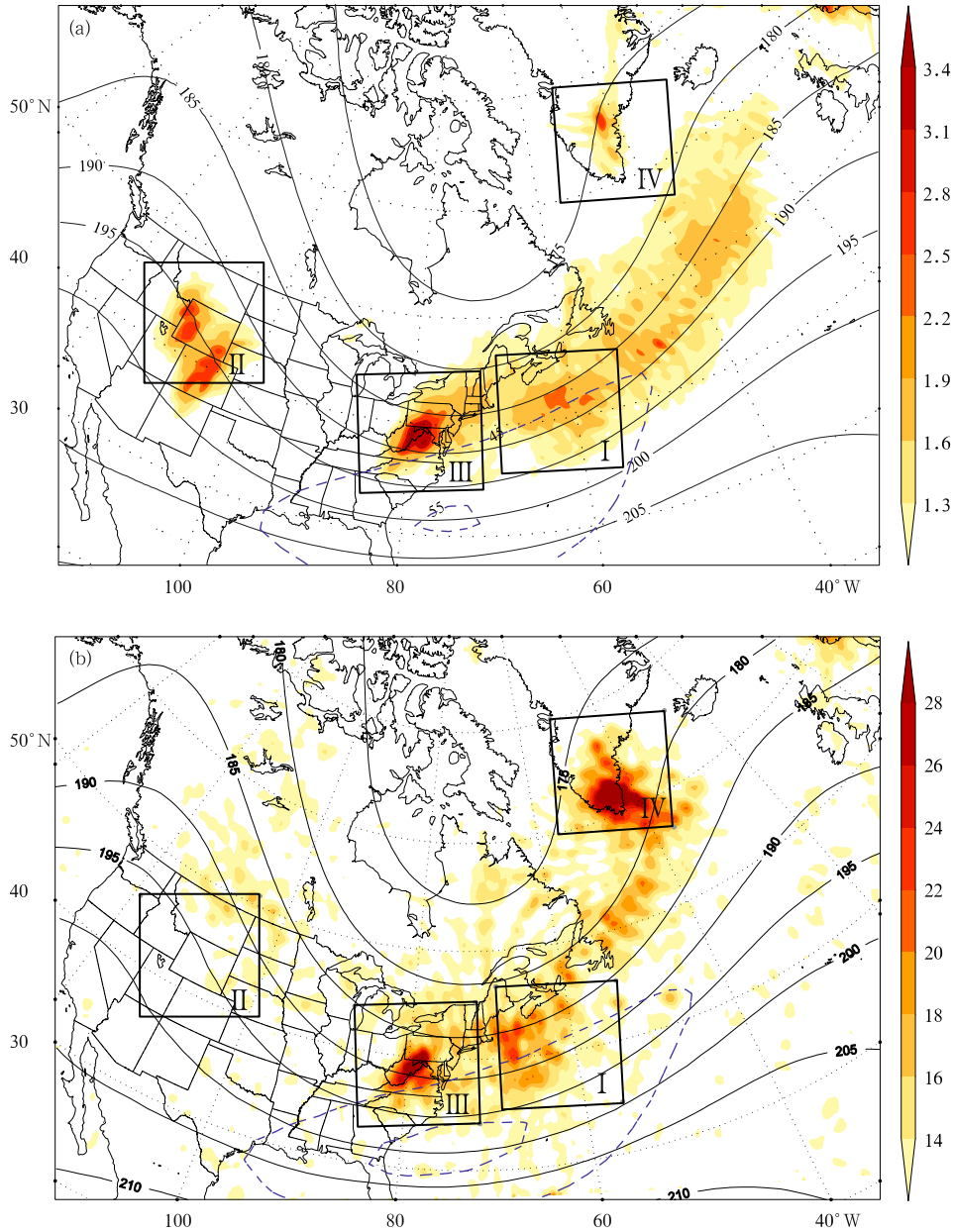


Fig. 1. (a) The 30-km MM5 model simulated monthly-mean GW KE at 21-km height (colored; $\Delta = 0.3 \text{ m}^2 \text{ s}^{-2}$) overlapped with pressure (solid; $\Delta = 5 \text{ hPa}$) and horizontal wind speed (dashed; only 45 and 55 m s^{-1} displayed) at 12-km height. (b) The AMSU-A channel-10 radiance variance (colored; $\Delta = 2 \text{ K}^2$) overlapped with the mean NCEP FNL analysis of pressure and wind speed (contoured as in (a)) at 12-km height. The inner rectangular boxes with numbers denote the locations of the four regions to be examined in Fig. 2.

$\times 1200 \text{ km}^2$ box. As for verification, the local variances of AMSU-A radiance of channel 9 are normalized and projected onto the equivalent model level (18 km) over corresponding areas (refers to Fig. 1). It is found that, over Region I, most of the jet-front GWs come from the GW event of 18–25 January, which are

confirmed both by the simulated KE and AMSU-A variance (Fig. 2a; also in Wu and Zhang, 2004). GWs over the Rockies are more persistent over the entire January, though significantly weaker in amplitude at higher altitude (Fig. 2b). Similar time evolution is seen in the AMSU-A variance at 18 km, but there are

some slight timing discrepancies for those weaker signals.

In contrast, enhanced GW variance is more episodic over the Appalachians and Greenland (Figs. 2c and 2d), where the topography is not as complicated as the Rocky Mountains, i.e., their terrain

roughness (Fritts and Nastrom, 1992) is mostly monodirectional: larger in the zonal direction but much smaller in the meridional direction. Therefore, the excitation of terrain-induced GWs over Regions III and IV may highly depend on the synoptic flow, which determines the strength of the cross-ridge wind (Kim et

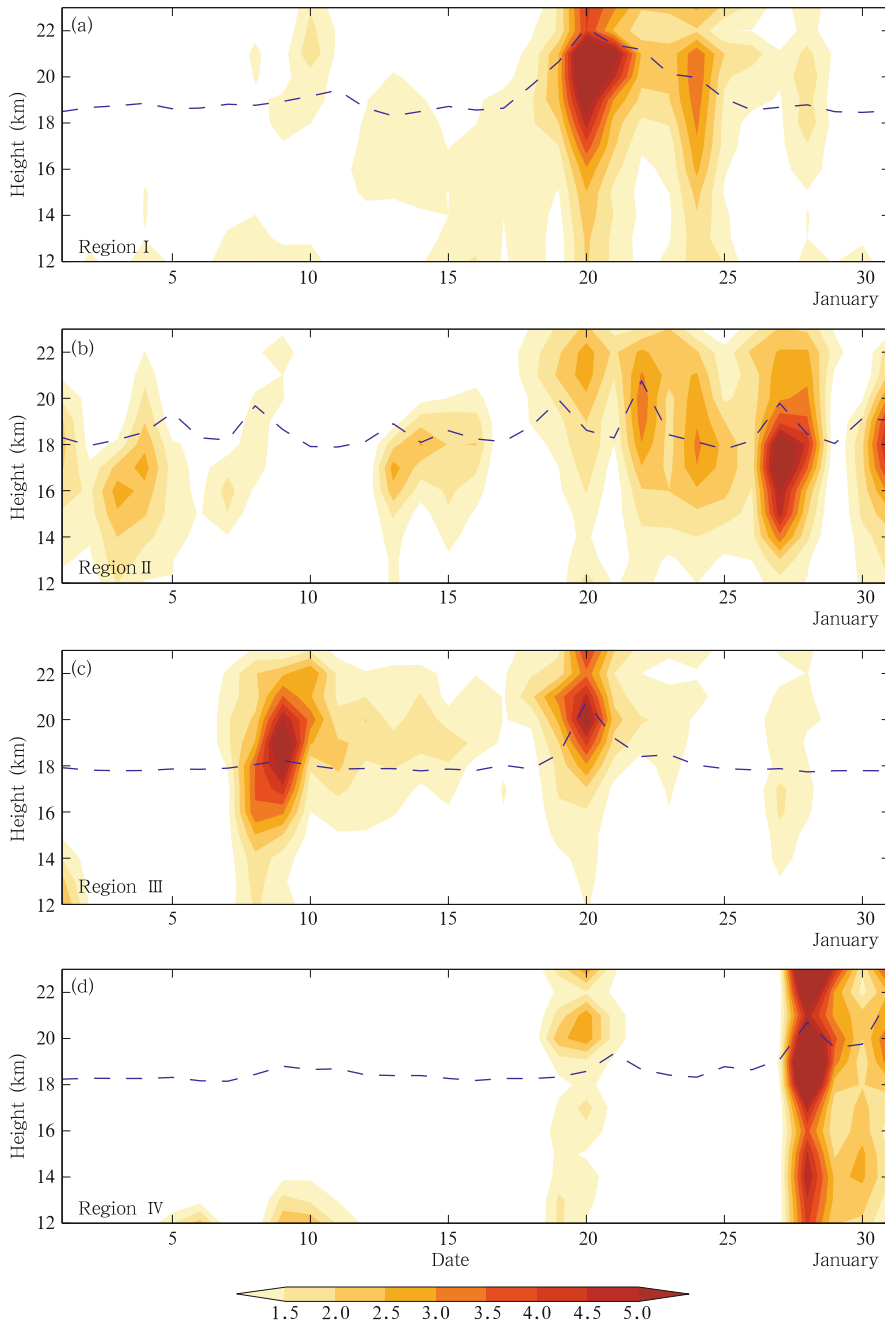


Fig. 2. Temporal and vertical variations of GW KE (colored; $\Delta = 0.5 \text{ m}^2 \text{ s}^{-2}$) averaged over the four box regions denoted in Fig. 1: (a) the northwestern Atlantic, (b) the Rockies, (c) the Appalachians, and (d) Greenland. The normalized AMSU-A radiance variance (dashed line) of channel 9 is projected at the equivalent height (18 km).

al., 2003). For instance, during 8–20 January, there was a major larger-scale trough over the East Coast of the U.S. travelling slowly eastward. After the northwest flow upstream of the trough dominated over the Appalachians with considerable cross-ridge component, significant amount of GW activities were produced during this period (Fig. 2c). The weak GW activities over Greenland are likely due to a slight mean jet-stream departure to the south compared with FNL analysis (Fig. 1b vs. Fig. 1a), implying a weaker cross-mountain flow in the simulation. On the other hand, the lack of strong AMSU-A variance in the Rocky region may be partially due to shorter wavelengths of the GWs that are hardly detectable in the coarse footprint of AMSU-A. In fact, enhanced GW activities over the Rockies have been reported in several previous studies using other types of measurements, e.g., aircraft data (Fritts and Nastrom, 1992), high-resolution radiosonde (Wang and Geller, 2003), and GPS occultation sounding (Tsuda et al., 2000). Our case-by-case investigations of model-derived wave characteristics found that GWs with a smaller wavelength (below 300 km) is prevalent over the Rocky Mountains. Hence, only small portions of the GWs may be captured by AMSU-A instruments, as speculated in Jiang et al. (2005).

4. Momentum fluxes of GW

Vertical flux of horizontal momentum produced by GWs could be deposited in the stratosphere and mesosphere, and plays important roles for maintaining general circulation and thermal structures, and mixing radiation-sensitive chemical species (Fritts and Alexander, 2003). The zonal and meridional components of the momentum fluxes are defined as $\overline{u'w'}$ and $\overline{v'w'}$, respectively. Figure 3 shows the simulated momentum fluxes of GWs with different wavelengths at 21-km height during the peak GW activities of 18–25 January 2003, where positive (negative) $\overline{u'w'}$ means eastward (westward), and positive (negative) $\overline{v'w'}$ means northward (southward), relative to the background flows for the upward-propagating GWs.

For mesoscale GWs with wavelength between 200

and 600 km in the 30-km simulations, strong westward zonal momentum transports (Fig. 3a) are found over most of the northwestern Atlantic regions and the Appalachians, where there are strong GW variances (Fig. 1). These GWs carry westward momentum fluxes in both regions with maximum value over $12 \times 10^{-2} \text{ m}^{-2} \text{ s}^{-2}$. In the meridional direction (Fig. 3d), relatively weaker southward momentum fluxes are found near the jet streaks, and contrarily, northward momentum fluxes are found over the Appalachians with reduced intensity/area compared to the zonal momentum flux. Similar amplitude and distribution of the wave fluxes for the GW wavelength between 200 and 600 km are also obtained in the 10-km simulations (figure omitted). Our simulation results are consistent with Sato et al. (1999) who suggested negative $\overline{u'w'}$ above the subtropical jets of the Northern Hemisphere using a coarse general circulation model (T106). We speculate that both sources and propagation may be responsible for the preferred direction of these momentum fluxes.

We further examine the resolved momentum fluxes of even smaller-scale GWs (with wavelength smaller than 200 km) in the 30-km simulations, and compare them with the 10-km simulations. A high-pass filter with 200-km cut-off wavelength is applied on the model-derived wind fields simulated by both the 30-km (Figs. 3b and 3e) and 10-km (Figs. 3c and 3f) simulations. It is shown that the 30-km grids failed to represent those smaller-scale GWs over the Atlantic region. The weaker amplitude of the zonal momentum flux over the Appalachians in Fig. 3b against Fig. 3c also indicates that the coarse domain could not completely describe those terrain-induced GWs with shorter wavelengths. This is consistent with Kuester et al. (2008), who showed abundant smaller-scale (15–300-km) GWs in their simulations with a horizontal grid spacing of 3 km, and also consistent with Kim et al. (2005), who showed that GWs with wavelength of 300–600 km prevailed in the 27-km simulations. It is worth noting that the center of zonal fluxes over the jet-front region in Fig. 3c (shorter waves) shifted slightly upstream compared to Fig. 3a (longer waves). These smaller-scale GWs are likely related to

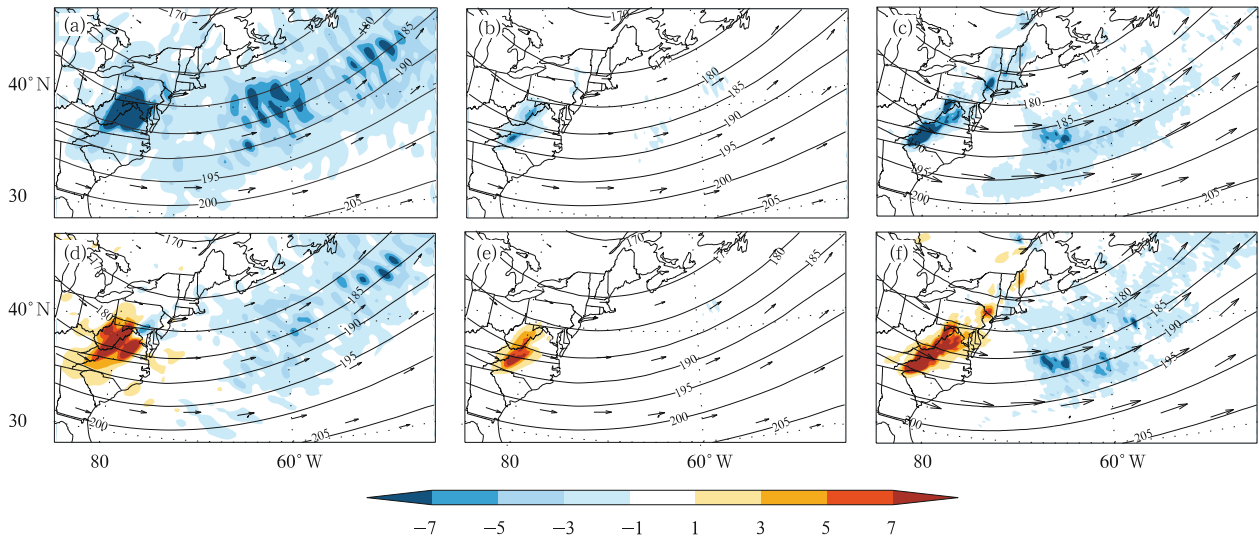


Fig. 3. The mean zonal (top panels) and meridional (bottom panels) momentum fluxes calculated at 21-km height during 18–25 January 2003 (colored; $\Delta = 2 \times 10^{-2} \text{ m}^2 \text{ s}^{-2}$) overlapped with pressure (solid line; $\Delta = 5 \text{ hPa}$) and horizontal winds (vector) at the same height. Panels (a) and (d) are for the GWs with wavelength of 200–600 km, and (b) and (e) are for the GWs with wavelength smaller than 200 km in the 30-km simulations. Panels (c) and (f) are for the GWs with wavelength smaller than 200 km in the 10-km simulations.

the lower-tropospheric origin of strong convections and surface fronts.

5. Sensitivity to spin-up time

Another topic of interest on the GW simulations is the sensitivity of wave amplitude and momentum

flux to model spin-up time. For example, inertial GWs excited by imbalance associated with the jet-front systems depend strongly on the background environments (Wang and Zhang, 2007), and are far from instant excitation assumed in most current-generation GW parameterization schemes. Figure 4 demonstrates the monthly mean maps of 21-km height KE valid at diffe-

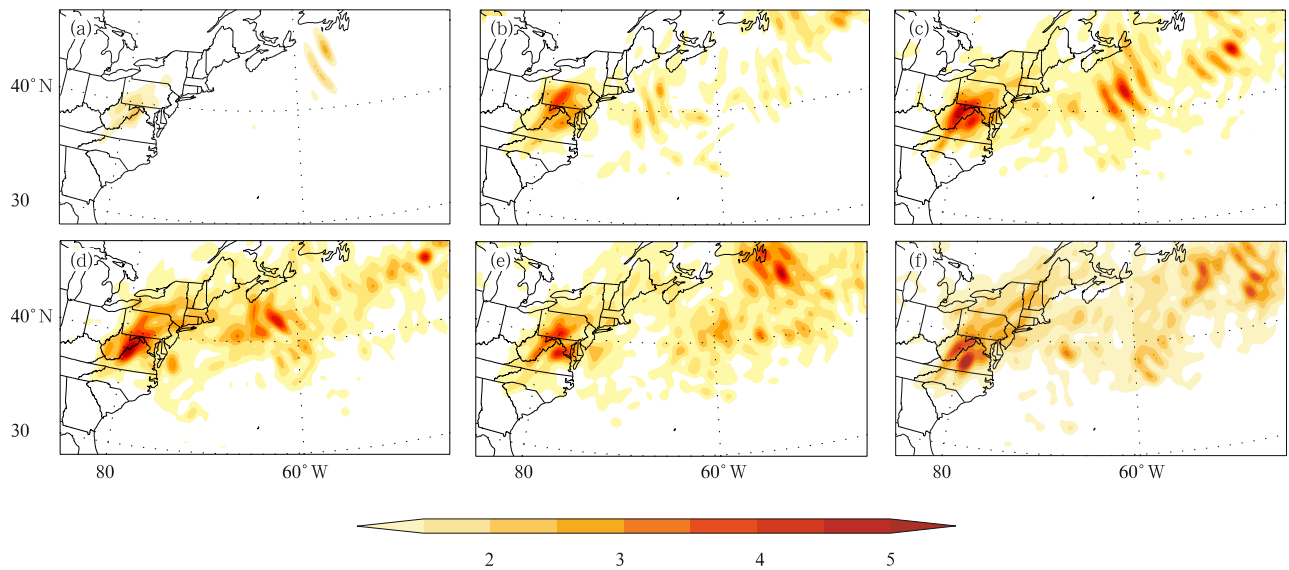


Fig. 4. The 30-km MM5 model simulated monthly-mean GW KE at 21-km height (colored; $\Delta = 0.5 \text{ m}^2 \text{ s}^{-2}$) calculated at different forecasting times: (a) 12 h, (b) 24 h, (c) 30 h, (d) 36 h, (e) 48 h, and (f) 54 h. The following panels are valid at the same time of the day: (a) and (d) for 0000 UTC, (b) and (e) for 1200 UTC, (c) and (f) for 1800 UTC.

rent lead times. Significant differences are found between the GW simulations with shorter and longer lead times, e.g., Figs. 4a–4f. Much weaker GW signals are produced in simulations with shorter lead times for both the jet-front and terrain-related GWs (Figs. 4a and 4b). We further examine the domain integrated KE at 12-km height versus lead time of forecast (figure omitted), which further suggests that KE saturates at 30 h. These comparisons show that it may take up to 30 h (about 2 inertial periods at 45 degree) for the mesoscale models to achieve reliable and consistent simulations of the GW signals¹. The time delay of enhanced GW activities also suggests that these waves are less likely from imbalance in the initial conditions; otherwise GWs would be apparent in the much earlier time (5–10 h) and decay away as initial adjustment is accomplished, as demonstrated in Fritts and Luo (1992). We speculate that the timing of wave generation and the duration of GWs propagation may both contribute to the sensitivity to the lead time.

6. Concluding remarks

Based on the month-long comparisons of the GWs from mesoscale model simulations and the AMSU-A radiance variance, four regions over North America and North Atlantic Ocean along the storm track are found to be preferred regions of strong GW activities, i.e., the northwestern Atlantic Ocean, the U.S. Rockies, the Appalachians, and Greenland. The first one may strongly relate to the midlatitude baroclinic jet-front system, and the others are all collocated with high topography. There are strong agreements in gravity wave intensity and its spatial/temporal distribution between mesoscale model simulations and satellite radiance estimates. However, the model simulated GWs are sensitive to model spin-up times. It is suggested that at least a 30-h spin-up time (about two inertial periods) is needed for mesoscale models in achieving consistency.

Consistent with previous observational and theoretical studies, momentum flux estimated from this month-long mesoscale simulations suggests that

mesoscale GWs carries strong westward momentum fluxes into the lower stratosphere from both the jet-front and topographic GWs. Since mesoscale processes and GWs cannot be resolved explicitly in the state-of-the-art general circulation models, their impact on larger-scale flow thus needs to be parameterized (Kim et al., 2003). It is essential to characterize the source mechanisms, phase/magnitude, and propagation of these GWs before we can fully assess their impacts on the general circulations (Fritts and Alexander, 2003; Plougonven and Zhang, 2013).

Acknowledgments. This contribution is dedicated to Professor Wu Rongsheng in celebration of his 60-yr career in meteorology and his 80th birthday. All authors are former students of Nanjing University who are very grateful to Professor Wu Rongsheng for his mentorship and inspiration on atmospheric dynamics that this study is related to. We also thank Wu Dong at NASA for his help on the use of the AMSU-A data. Comments by two anonymous reviewers on an earlier version of the manuscript are helpful in the revision.

REFERENCES

- Alexander, M., M. Geller, C. McLandress, et al., 2010: Recent developments in gravity-wave effects in climate models and the global distribution of gravity-wave momentum flux from observations and models. *Quart. J. Roy. Meteor. Soc.*, **136**(650), 1103–1124.
- Allen, S. J., and R. A. Vincent, 1995: Gravity wave activity in the lower atmosphere: Seasonal and latitudinal variations. *J. Geophys. Res.*, **100**(D1), 1327–1350.
- Bei, N. F., and F. Q. Zhang, 2007: Impacts of initial condition errors on mesoscale predictability of heavy precipitation along the Mei-Yu front of China. *Quart. J. Roy. Meteor. Soc.*, **133**(622), 83–99.
- Blumen, W., and R. S. Wu, 1995: Geostrophic adjustment: Frontogenesis and energy conversion. *J. Phys. Oceanogr.*, **25**(3), 428–438.
- Fritts, D. C., and Z. G. Luo, 1992: Gravity wave excitation by geostrophic adjustment of the jet stream. Part I: Two-dimensional forcing. *J. Atmos. Sci.*, **49**(8), 681–697.

¹ The 30-h spin-up time (and KE amplitude) is also consistent with the saturation time scale of mesoscale error energy (and imbalance) in the mesoscale predictability study of Bei and Zhang (2007) and Zhang et al. (2007).

- , and G. D. Nastrom, 1992: Sources of mesoscale variability of gravity waves. Part I: Topographic excitation. *J. Atmos. Sci.*, **49**(2), 101–110.
- , and M. J. Alexander, 2003: Gravity wave dynamics and effects in the middle atmosphere. *Rev. Geophys.*, **41**(1), 1003–1063.
- Grell, G. A., J. Dudhia, and D. R. Stauffer, 1994: A description of the fifth-generation Penn State/NCAR Mesoscale Model (MM5). Tech. Note TN-3981IA, National Center for Atmospheric Research, Boulder, CO, 125 pp.
- Jiang, J. H., S. D. Eckermann, D. L. Wu, et al., 2005: Seasonal variation of gravity wave sources from satellite observation. *Adv. Space Res.*, **35**(11), 1925–1932.
- Kim, S.-Y., H.-Y. Chun, and J.-J. Baik, 2005: A numerical study of gravity waves induced by convection associated with Typhoon Rusa. *Geophys. Res. Lett.*, **32**(24), L24816, doi: 10.1029/2005GL024662.
- Kim, Y.-J., S. D. Eckermann, and H.-Y. Chun, 2003: An overview of the past, present and future of gravity-wave drag parametrization for numerical climate and weather prediction models. *Atmos. Ocean*, **41**(1), 65–98.
- Kuester, M. A., M. J. Alexander, and E. A. Ray, 2008: A model study of gravity waves over Hurricane Humberto (2001). *J. Atmos. Sci.*, **65**(10), 3231–3246.
- Plougonven, R., and F. Q. Zhang, 2013: Internal gravity waves from atmospheric jets and fronts. *Rev. Geophys.*, in review.
- Powers, J. G., and R. J. Reed, 1993: Numerical simulation of the large-amplitude mesoscale gravity-wave event of 15 December 1987 in the central United States. *Mon. Wea. Rev.*, **121**(8), 2285–2308.
- Sato, K., T. Kumakura, and M. Takahashi, 1999: Gravity waves appearing in a high-resolution GCM simulation. *J. Atmos. Sci.*, **56**(8), 1005–1018.
- Shutts, G. J., and S. B. Vosper, 2011: Stratospheric gravity waves revealed in NWP model forecasts. *Quart. J. Roy. Meteor. Soc.*, **137**(655), 303–317.
- Tsuda, T., M. Nishida, C. Rocken, et al., 2000: A global morphology of gravity wave activity in the stratosphere revealed by the GPS occultation data (GPS/MET). *J. Geophys. Res.*, **105**(D6), 7257–7274.
- Uccellini, L. W., and S. E. Koch, 1987: The synoptic setting and possible energy sources for mesoscale wave disturbances. *Mon. Wea. Rev.*, **115**(3), 721–729.
- Wang, L., and M. A. Geller, 2003: Morphology of gravity-wave energy as observed from 4 years (1998–2001) of high vertical resolution U.S. radiosonde data. *J. Geophys. Res.*, **108**(D16), 4489–4496.
- Wang, S. G., and F. Q. Zhang, 2007: Sensitivity of mesoscale gravity waves to the baroclinicity of jet-front systems. *Mon. Wea. Rev.*, **135**(2), 670–688.
- Wu, D. L., 2004: Mesoscale gravity wave variances from AMSU-A radiances. *Geophys. Res. Lett.*, **31**(12), L12114, doi: 10.1029/2004GL019562.
- , and F. Q. Zhang, 2004: A study of mesoscale gravity waves over the North Atlantic with satellite observations and a mesoscale model. *J. Geophys. Res.*, **109**, D22104, doi: 10.1029/2004JD005090.
- Zhang, F. Q., 2004: Generation of mesoscale gravity waves in upper-tropospheric jet-front systems. *J. Atmos. Sci.*, **61**(4), 440–457.
- , C. A. Davis, M. L. Kaplan, et al., 2001: Wavelet analysis and the governing dynamics of a large-amplitude mesoscale gravity-wave event along the East Coast of the United States. *Quart. J. Roy. Meteor. Soc.*, **127**(577), 2209–2245.
- , S. E. Koch, and M. L. Kaplan, 2003: Numerical simulations of a large-amplitude mesoscale gravity wave event. *Meteor. Atmos. Phys.*, **84**(3–4), 199–216.
- , N. F. Bei, R. Rotunno, et al., 2007: Mesoscale predictability of moist baroclinic waves: Convection-permitting experiments and multistage error growth dynamics. *J. Atmos. Sci.*, **64**(10), 3579–3594.